Resonance vibration of amorphous SiO_2 nanowires driven by mechanical or electrical field excitation

D. A. Dikin, X. Chen, W. Ding, G. Wagner, and R. S. Ruoff[a)]
Department of Mechanical Engineering, Northwestern University, Evanston, Illinois 60208-3111

(Received 24 May 2002; accepted 16 October 2002)

In this work, we have used the mechanical resonance method to determine the bending modulus of amorphous SiO_2 nanowires and to study an electron charge trapping effect that occurs in these nanowires. For uniform *amorphous* nanowires having diameter ~100 nm and length over 10 μm, the fit modulus values cluster near 47 GPa; this value is lower than the commonly accepted value of ~72 GPa for fused silicon oxide (glass) fibers. For some SiO_2 nanowires, we observed up to three closely spaced resonances that are a result of the nanowire anisotropy. We have compared the resonance vibration of nanowires driven by mechanical and also ac electrical field loading. All of the measurements were done inside the chamber of a scanning electron microscope where the nanowires were under bombardment of a flux of ~3 keV energy electrons. By watching the interaction between the ac electrical field and exposed nanowire when driven at resonance frequency, we have observed significant charge trapping in the nanowires. The combination of charge trapping and decay time was nonuniformly distributed along the nanowire. This suggests a nondestructive method that can be used for studying defects in certain types of nanostructures.
 [DOI: 10.1063/1.1527971]

I. INTRODUCTION

Use of a driving electrical field to excite mechanical resonance in nanostructures is a simple, compact, and controllable method that can be utilized in sensors and actuators. The ac electric-field excitation of the mechanical vibration of a nanowire (NW) at its fundamental resonance frequency, in particular, has been used in the past few years in determining the elastic parameters of synthesized quasione-dimensional nanosize rods, tubes, and whiskers.[1–4] Such work has focused on resonant excitation of naturally cantilevered filaments residing in a sample, so a direction for future work would be to grow nanostructures where desired so that they are perfectly aligned for applications.

The electronic and mechanical properties of amorphous inorganic materials are less predictable and more difficult to analyze than crystalline materials. The types of defects present are rather difficult to detect compared with dislocations or grain boundaries in crystalline materials, and the correlation of properties with structure and defects can benefit from methods such as the measurement of charge trapping and dissipation, in addition to direct structural analysis. Photoluminescence, defect formation, and defect centers have been studied in different types of silicas[5] and in amorphous silicon dioxide[6] in thin-film form, with the goal of achieving a better understanding for a variety of applications, such as in submicron optics and different optoelectronic devices.

Recently, amorphous silicon oxide NW's have been synthesized by several groups.[7,8] Here, we will discuss our results on the coupling of mechanical and electrical behaviors in amorphous SiO_2 NW's. This work opens directions for characterizing the electromechanical response of nonmetallic nanowires, and for studying the interaction of electrons with such NW's.

II. MATERIAL AND EXPERIMENTAL TECHNIQUE

The SiO_2 NW's were synthesized in a horizontal tube furnace via a vapor–liquid–solid process using molten Ga as the catalyst and a silicon wafer as the Si source. The experimental setup and synthesis procedure were reported in detail in Ref. 8. Highly aligned SiO_2 NW's with diameters from 50 to 100 nm and lengths from 10 to 50 μm were obtained in high yield after a 5 h growth. Most of these NW's are joined along some portion of their length (see Fig. 1). They are amorphous according to electron diffraction obtained by transmission electron microscopy (TEM) (Hitachi HF-2000) and are composed of only Si and O with an atomic ratio of about 1:2 as measured by electron energy-loss spectrometry (EELS). A high-resolution TEM (HRTEM) image and electron diffraction pattern are shown in Fig. 1.

Our initial goal was to measure the bending modulus of the amorphous SiO_2 NW's by using the natural resonance vibration method of a cantilevered beam. An easy way to apply periodic loading is by excitation with an ac electrical field. An alternative method is to mechanically drive the NW holder, and thus the NW.

Two sharp scanning tunnel microscope (STM) tips were bonded onto two opposite positioning stages for NW manipulation and also used as conductive leads. One of the STM cantilevers was bonded onto a piezoelectric bimorph actuator. By applying an ac voltage to this piezoactuator, the STM tip with an attached NW can be driven in mechanical vibration.

[a)]Author to whom correspondence should be addressed; electronic mail: r-ruoff@northwestern.edu

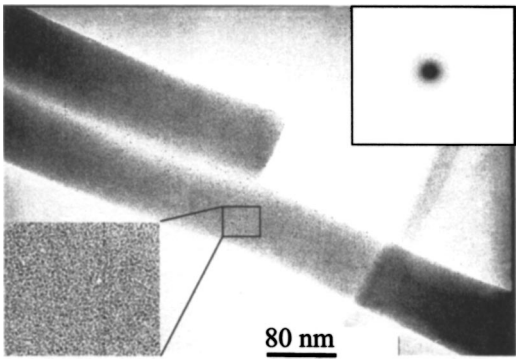

FIG. 1. TEM image of SiO_2 NW. HRTEM image (inset in lower left-hand side corner) and the electron diffraction pattern (inset in upper right-hand side corner) demonstrate that these NW's are amorphous.

In both electrical and mechanical excitations, we used a function generator as an ac voltage source (SRS model DS345) both with and without dc bias, with the frequency swept up to 30 MHz. Figure 2(a) shows the schematic of the experimental setup. A homemade nanomanipulator having X, Y, Z, and rotational degrees of freedom[9] was used to approach individual NW's, and all aspects of the experiment were directly imaged inside a scanning electron microscope (SEM) (Hitachi S4500 FEG SEM). Individual NW's can be picked up, attached, and driven into resonance by these different methods during one experimental session.

Initially, a sample of NW's was placed onto a metal wire that sometimes was covered with conductive carbon tape for better adhesion. This metal wire was then attached to the manipulator and, in some preliminary experiments, this was used as one of the electrodes. Experience showed that the aggregation of NW's made it difficult to determine the length of individual NW's and also the nature of the attachment of the NW. Inaccuracy in these parameters can lead to an order-of-magnitude error in the value of the calculated bending modulus. Consequently, we altered our approach and for the studies reported here, maneuvered the STM tip into the agglomeration of NW's to pull out individual ones for measurement.

The frequency of the NW vibration was always much larger than the SEM raster scanning. Thus, the NW resonance frequency and the amplitude of the NW vibration can be measured by using a secondary-electron detector of the SEM in the ''spot'' and ''line'' modes and the amplitude can be also measured by video recording followed by further image processing. In the spot mode, the electron beam is stopped on one point and the frequency of the oscillating nanostructure is detected by the modulation of intensity of the secondary-electrons arriving at the secondary electron detector. In the line scan mode, a single line from the normal rastering of the electron beam is used to measure the amplitude of the oscillating structure at a given location along the NW.

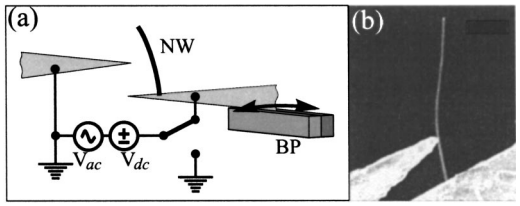

FIG. 2. (a) Schematic of the experimental setup: Electrode on the right-hand side holds a NW and is fixed at the end of bimorph piezodriver. (b) SEM micrograph shows a SiO_2 NW clamped to one electrode and touched by another probe.

Imaging was typically done with a 3 keV electron-beam energy, the electron energy for which we found the highest imaging resolution. This fact agrees well with basic theory of the electron–specimen interaction for SiO_2.[10]

III. RESULTS AND DISCUSSION

A. Bending modulus

As just mentioned, two methods for driving mechanical resonance of the SiO_2 NW's were used. For a uniform circular cross section cantilever beam, which has one end ideally clamped and the second end free, the simple beam theory[11] for flexural vibration gives the natural resonance frequency as:

$$f_n = \frac{\beta_n^2}{2\pi}\frac{d}{L^2}\sqrt{\frac{E}{16\rho}}. \tag{1}$$

Here β_n is the eigenvalue obtained from the characteristic equation $\cosh(\beta_n)\cos(\beta_n) = -1$, d is the diameter, L is the length of the NW, E is the modulus of elasticity, and ρ is the material density. In our experiments, we saw only the fundamental mode of vibration, which corresponds to the first eigenvalue $\beta_0 = 1.875$. It is likely that higher modes could not be excited for several reasons. We find that it is not possible to excite higher-order modes when the aspect ratio L/d of the SiO_2 NW's is below ~ 200, possibly because the excitation power was not high enough. According to beam theory,[11] the normalized amplitude of vibration (y_n) along the beam (x axis) is given by:

$$y_n(x) = \cosh\beta_n x - \cos\beta_n x - \left(\frac{\sinh\beta_n - \sin\beta_n}{\cosh\beta_n + \cos\beta_n}\right) \cdot (\sinh\beta_n x - \sin\beta_n x), \tag{2}$$

where x is normalized with respect to the length L of the beam.

A typical example is shown in Fig. 3, where we can see the nanowire vibration at its fundamental frequency driven by the ac electrical field [Fig. 3(b)], and the calculated displacement [Fig. 3(c)]. The longitudinal distribution of stiffness can be assessed by the relationship between the measured and calculated shapes. While the measured wire is not perfectly straight and uniform the rough agreement between the real and calculated shapes in Fig. 3 suggests that the stiffness is essentially uniform along the entire length of the NW.

One of the studied NW's was measured for about 8 h during four SEM sessions and was driven in vibration for $\sim 10^9$ cycles. For these 8 h, the spot and line modes were not used—the NW was imaged in normal raster mode. This SiO_2 NW thus displayed a durable mechanical response without any change of its resonance characteristics. Finally, during

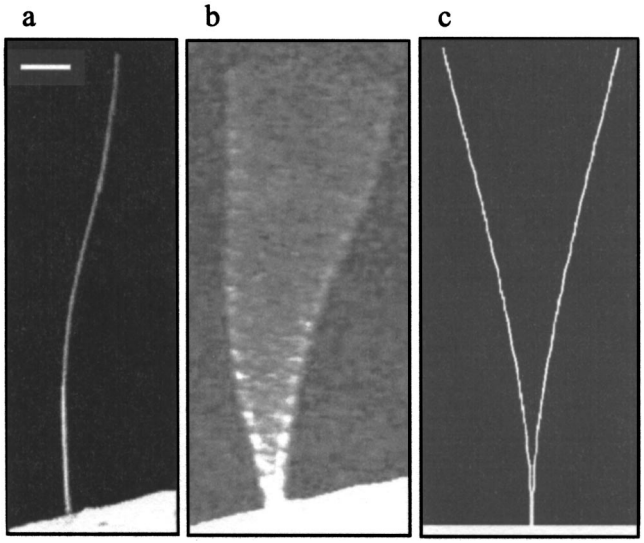

FIG. 3. (a) SEM micrograph of a clamped-free SiO_2 NW that is 18.9 μm long and 110 nm in diameter (scale bar is 2 μm long). (b) Vibration of the same NW as driven by an ac electric field. (c) The calculated shape of the first vibrational mode of a cantilevered beam of these dimensions.

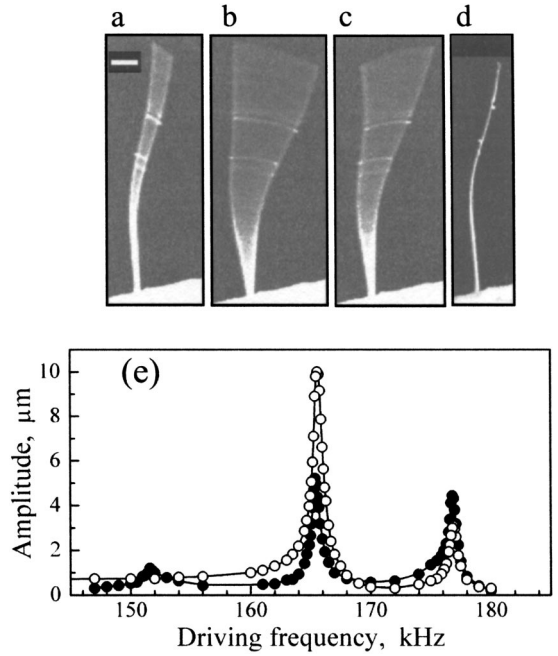

FIG. 4. A SiO_2 NW driven mechanically at three closely spaced resonant frequencies (a, b, and c). This is the same NW as shown in Fig. 3, however, now having attached nanoparticles (d). The corresponding amplitude vs frequency curves are shown in (e). The SEM micrographs (a, b, and c) show mechanically driven modes whereas the amplitude vs frequency curves are shown for both mechanically (solid circles) and electrically (open circles) driven modes (e). The Q factor was about 80 for all cases. Scale bar in SEM micrograph is 2 μm long.

the last session of experiments, we focused the electron beam to a tight spot on the end of this NW, and this caused the NW to curve [see the top section of the NW in Fig. 4(d)]. Perhaps this was due to the electron flux density increasing by a factor of $\sim 10^4$ (up to $\sim 10^4$ A/m^2). For low atomic number materials, it is known[10] that a significant fraction of the primary electron-beam energy is transformed into heat in the specimen.

During the last SEM session for this particular SiO_2 NW, we found three nanosized particles [see Fig. 4(d)] asymmetrically attached at different locations around the perimeter. This additional mass caused a significant shift of frequency from 186.5 kHz to the lower resonance frequencies (176.8, 165.4, and 151 kHz). This triple-resonance response was seen when the NW was driven mechanically (through the piezo attached to the STM tip holding the NW) and two resonances (165.4 and 176.8 kHz) were observed when the NW was driven by the ac electrical field method. Image blurring due to the applied ac voltage for the electrical excitation case completely masked the smallest amplitude of vibration, which occurs at the lowest frequency 151 kHz, observed by the mechanical excitation method. The amplitude–frequency characteristics for both types of excitation are shown in Fig. 4(e). As can be seen in Figs. 4(a)–4(c), all three closely spaced mechanically driven resonances have different orientations, apparently representing slightly different torsional motion of the oscillated wire. Furthermore, for the two resonances where the frequencies were identical for mechanical and electrical driving (165.4 and 176.8 kHz), the orientations of each respective mode (mechanical versus electrical at 165.4 kHz, and mechanical versus electrical at 176.8 kHz) were identical, but the amplitudes were different.

Closely spaced resonances have also been observed by other researchers[12] in resonating carbon nanotubes. This may be due to the anisotropy of the nanostructure, either in material properties (elastic modulus or density) or geometry (cross-sectional area, crooked beam). This anisotropy may also result in the different planes of the NW motion, which are clearly seen in Figs. 4(a)–4(c). Modeling of this phenomenon is suggested as an area for future work.

The calculated values for the bending modulus of three SiO_2 NW's are shown in Table I. The density of the amorphous SiO_2 NW's is assumed to be 2.2×10^3 kg/m^3.[13] The accuracy of the calculated modulus is mostly determined by the accuracy of the measurement of the dimensions of the NW, and by the assumption that the use of the continuum beam formula is valid.

The quality (Q) factors measured for these NW's ranged from 70 to 250. We note, in Fig. 4(e), that the Q in our experiments was essentially the same for mechanical and electrical excitations. One of the reasons for such a low Q is likely the amorphous structure of these NW's. Another possible cause of frequency broadening for the resonance curve is the presence of a substantial axial load component. In these experiments, the external electrical field was primarily directed along the long axis of the NW, rather than perpen-

TABLE I. Bending modulus of SiO_2 NW's.

Length (μm) ($\pm$0.2)	Diameter (nm) ($\pm$5)	Natural frequency (kHz)	E (GPa)
17	80	172.0	43.4$\pm$7.0
17.3	88	193.8	48.8$\pm$7.8
18.3	98	190.0	47.4$\pm$8.4

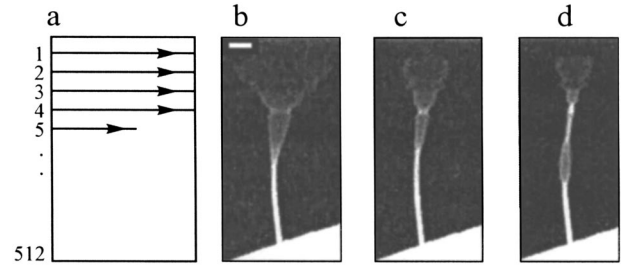

FIG. 5. "Strange" shapes of the vibrated NW obtained at three different scan modes of the SEM, together with a schematic representation of the scanning electron beam (a). (b) Time interval between each closed scan line inside of one frame is: (b) 4 ms, (c) 17 ms, and (d) 50 ms. All three images were taken under the same experimental conditions: Frequency and amplitude of ac field, counterelectrode position, energy, and density of electron flux in SEM. The difference is only the sweep rate that results in a different time of irradiation and time break between the subsequent interactions of electron-beam and wire.

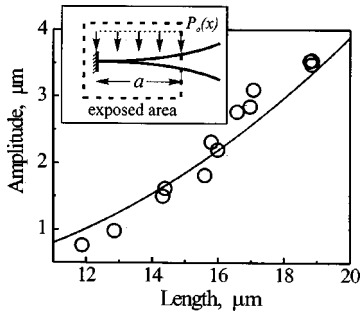

FIG. 6. Measured (open circles) and calculated (solid line) dependencies of the amplitude of the NW deflection at some fixed point vs the length of the wire a, which is assumed to be under the loading force $P_0(x)$. Vibration of the NW excited by the ac electric field. Inset shows schematic of the measurements; the dashed rectangle corresponds to the size of the area exposed to the electron flux. According to our simple model, the ac loading force is evenly distributed along the length of a, and is zero outside this section length.

dicular to it. The same was true for the mechanical driving. The force of inertia has its largest component along the long-axis direction because the NW's are essentially aligned along the direction of bimorph motion. Therefore, cyclical variation in the axial load, which is tensile in one half period and compressive the next, may lead to losses in the energy of the fundamental mode of vibration due to a small deformation in the axial direction, as well as through nonlinearities caused by the axial direction inertia. An exciting area for future research is to identify and elucidate the intrinsic loss mechanisms for both mechanical and electrical excitations of these, and other, NW's.

B. Charge trapping

The Hitachi S-4500 SEM has a variety of imaging modes. We briefly explain these because it is relevant to the focus of this section. "TV mode" (of which there are two raster speeds; when we refer to TV mode we refer to using the fastest raster scan, namely 63.5 μs for each line) was used in our early work to image both the mechanical and electrical excitations of resonance. In this high scan rate mode, the resonances were identical. When we decided to obtain high-resolution and contrast images, we attempted to use "photorecording mode," which has a time of 68 ms for each line. The image looked quite different compared to what had been viewed in TV mode. This led us to experiment with some intermediate rastering rates in the "viewing mode" (of which TV mode is the fastest), such as 0.72, 4, 17, and 50 ms for each line, and the images that result (for 4, 17, and 50 ms) are shown in Fig. 5.

As Fig. 5 shows, for these lower scan rates, the scan rate influences the resonance response of the electrically excited NW. We checked to see if these slower scan rates influenced the mechanically excited NW, but there was no dependence on scan rate. This suggested to us that at these lower scan rates, there is an unequal distribution of charges and that this plays a major role in the interaction between the SiO_2 NW and the external ac electric field.

In order to test this hypothesis, we used TV mode to measure the NW amplitude of the vibration as a function of a section length (measured from the clamped side of the NW) of the NW that was exposed to the electron-beam flux from the SEM. That is, the exposed section length varied from 11.9 to 18.9 μm, which was a total cantilever length L. A schematic of this experiment is shown in the inset of Fig. 6.

We then assumed that this section, having length a (where a varied from 11.9 to 18.9 μm), is the only part of the NW where force is applied. The dependence of the amplitude of the vibration on a can be computed if we assume that the force $P_0(x)$ is evenly distributed over this charged section. The amplitude of motion A for the fundamental mode shape should be proportional to the mathematical projection of the force onto the fundamental mode. Letting $P_0(x)=P$ for $0 \leqslant x \leqslant a$, where P is a constant, and $P_0(x)=0$ for $a<x\leqslant L$, gives

$$A \propto \int_0^L P_0(x) y_0(x)\,dx, \qquad \propto P \int_0^a y_0(x)\,dx, \tag{3}$$

where $y_0(x)$ is the fundamental mode shape given by Eq. (2), with $\beta_0 = 1.875$. Evaluation of Eq. (3) yields

$$A = P^*\{0.783 - 0.391[\cos(\beta_0 a/L) + \cosh(\beta_0 a/L)] - 0.533[\sin(\beta_0 a/L) - \sinh(\beta_0 a/L)]\}, \tag{4}$$

where P^* is a constant of proportionality. The measured amplitude of the vibration and the calculated dependence as a function of the exposed length [Eq. (4)] are shown in Fig. 6. Figure 6 suggests that this simple model is correct: Charging of the exposed section leads to the ac electrical field applying load only on that section of the length.

It is well known that electron bombardment can locally charge insulators. Charge trapping by conducting or insulating materials under electron bombardment has been studied experimentally and theoretically (see Ref. 14 for a review). The buildup of localized charge in amorphous SiO_2 under low-energy electron bombardment (0.1 to 10 keV) has been reported by Vigouroux *et al.*[15] These authors demonstrated

that the charge trapping sites are defects induced by the electron beam, despite the fact that the energy absorption per implanted electron (by direct transfer of momentum) is much less than the energy of the silicon–oxygen bond. Defect creation was attributed to a radiolytic process[16] whereby an oxygen atom is moved from its normal bonding position to an adjacent split bonding position. The latter configuration normally decays in milliseconds or less.[16,17] Their conclusion about the decay time scale is relevant to our experiments.

The time interval of 63.5 μs per scan line in TV mode when the NW is electrically driven evidently keeps the NW equally charged along its length, and the resulting NW vibration has the same shape as would be caused by mechanical driving [see Figs. 3(b) and 4(b)]. Whenever the SEM scanning mode is slowed down to, for example, 0.72 ms between the scan lines (mode 1 in the ''viewing mode''), the exposed zones of the NW have time to partially dissipate their charges, resulting in a smaller applied load and a smaller amplitude of the wire deflection; in addition, the image is clearly suggestive of an uneven distribution of charge along the NW.

Thus, we report a simple method to map this charging effect and its decay time as a function of position along the length of the cantilevered NW. We emphasize that the SiO_2 NW diameter was only ~ 5 times larger than the mean-free path of the secondary electrons in amorphous bulk SiO_2. As a consequence of the strong interaction of the 3 keV primary electrons with these types of specimens, the whole cross section of the nanostructure can be probed.

IV. CONCLUSION

We have fit the bending modulus of amorphous SiO_2 NW's by using the resonance vibration method. We often observed closely spaced resonances that likely result from slight anisotropy in the NW's, and, in one particular case, the anisotropy was identified as three attached particles. Low-energy electron bombardment of amorphous SiO_2 NW's can lead to significant charge trapping at particular points along the wire. This suggests a nondestructive method that can be used for studying defects, charge trapping, and charge dissipation in certain types of nanostructures.

ACKNOWLEDGMENTS

Scanning and transmission electron microscopy imaging was done at the Electron Probe Instrumentation Center at Northwestern University. TEM imaging was done by Yan Li. The work was supported from the NASA Langley Research Center Computational Materials: Nanotechnology Modeling and Simulation Program and by ONR Miniaturized Intelligent Sensors program (2001 funding), and by prior NSF support for building the SEM nanomanipulation stage (New Methods and Tools for Nanotechnology, NSF-DMR No. 9871874).

[1] P. Poncharal, Z. L. Wang, D. Ugarte, and W. A. de Heer, Science **283**, 1513 (1999).
[2] R. Gao, Z. L. Wang, Z. Bai, W. A. de Heer, L. Dai, and M. Gao, Phys. Rev. Lett. **85**, 622 (2000).
[3] Z. L. Wang, R. P. Gao, P. Poncharal, W. A. de Heer, Z. R. Dai, and Z. W. Pan, Mater. Sci. Eng., C **16**, 3 (2001).
[4] J. Fujita, M. Ishida, T. Sakamoto, and Y. Ochiai, J. Vac. Sci. Technol. B **19**, 2834 (2001).
[5] H. Nishikawa, T. Shiroyama, R. Nakamura, Y. Ohki, K. Nagasawa, and Y. Hama, Phys. Rev. B **45**, 586 (1992).
[6] C. Itoh, T. Suzuki, and N. Itoh, Phys. Rev. B **41**, 3794 (1990).
[7] B. Zheng, Y. Wu, and J. Liu, Adv. Mater. **14**, 122 (2002).
[8] Z. W. Pan, Z. R. Dai, C. Ma, and Z. L. Wang, J. Am. Chem. Soc. **124**, 1817 (2002).
[9] M.-F. Yu, M. J. Dyer, G. D. Skidmore, H. W. Rohrs, X. K. Lu, K. D. Ausman, J. R. Von Ehr, and R. S. Ruoff, Nanotechnology **10**, 244 (1999).
[10] J. I. Goldstein *et al.*, *Scanning Electron Microscopy and X-Ray Microanalysis* (Plenum, New York, 1992), Chap. 3.5.1.
[11] S. Timoshenko, *Theory of Elastic Stability* (McGraw–Hill, New York, 1936); R. E. D. Bishop and D. C. Johnson, *Mechanics of Vibration* (Cambridge University Press, Cambridge, U.K., 1960).
[12] M.-F. Yu, G. J. Wagner, and M. J. Dyer (private communication).
[13] T. Campbell, R. K. Kalia, A. Nakano, F. Shimojo, K. Tsuruta, and P. Vashishta, Phys. Rev. Lett. **82**, 4018 (1999).
[14] W. S. M. Werner, Surf. Interface Anal. **31**, 141 (2001).
[15] J. P. Vigouroux, J. P. Duraud, A. Le Moel, C. Le Gressus, and D. L. Griscom, J. Appl. Phys. **57**, 5139 (1985).
[16] K. Tanimura, T. Tanaka, and N. Itoh, Phys. Rev. Lett. **51**, 423 (1985).
[17] W. Hayes, M. J. Kane, O. Salminen, R. L. Wood, and S. P. Doherty, J. Phys. C **17**, 2943 (1984).